JMEPEG (2010) 19:155–165
DOI: 10.1007/s11665-009-9389-7

1059-9495/$19.00

Influences of Welding Processes on Microstructure, Hardness, and Tensile Properties of AZ31B Magnesium Alloy

G. Padmanaban, V. Balasubramanian, and J.K. Sarin Sundar

(Submitted September 12, 2008; in revised form January 24, 2009)

This article reports the influences of welding processes such as gas tungsten arc welding (GTAW), friction stir welding (FSW), and laser beam welding (LBW) on tensile properties of AZ31B magnesium alloy. The lowest hardness distribution profile (LHDP) is constructed across the weld section to identify the fracture path. From this investigation, it is found that LBW joints exhibited superior tensile properties compared to GTAW and FSW joints and this is mainly due to the formation of very fine grains in the fusion zone and absence of heat-affected zone (HAZ).

Keywords friction stir welding, gas tungsten arc welding, laser beam welding, magnesium alloy, tensile properties

1. Introduction

Magnesium (Mg) alloys have recently received considerable attention because of their excellent properties such as light weight, high specific strength and stiffness, machinability, and recyclability. These advantages make magnesium alloys very attractive materials in a wide variety of applications, where weight reduction is extremely important (Ref 1).The electronics and consumer goods industries are also responding to the widening acceptance of magnesium alloys. However, magnesium alloys are still not as popular as aluminum alloys in structural applications, and a major technical challenge is the development of reliable and inexpensive joining methods to produce high-quality welds. The welding of magnesium alloys, though not very difficult, needs precautionary measures, since they have a wide solidification range and form brittle intermetallic phases (Ref 2-4).

Gas tungsten arc welding (GTAW) of magnesium alloys produces some defects such as porosity and hot crack, which deteriorate their mechanical properties. The production of the defect-free weld requires complete elimination of the surface oxide layer and selection of suitable welding parameters. Although reasonable welding speeds can be achieved, some problems can be experienced such as high-welding residual stresses and changes in microstructure resulting from melting and solidification. High-purity shielding gases are necessary to prevent weld contamination; magnesium alloys can readily oxidize in the weld zone because of their high-chemical reactivity at high temperatures (Ref 5). Friction stir welding (FSW) is capable of joining magnesium alloys without melting and thus it can eliminate problems related to the solidification. As FSW does not require any filler material, the metallurgical problems associated with it can also be reduced and good quality weld can be obtained (Ref 6). LBW is particularly attractive for innovative and cost-effective applications, which require high precision, and processing speed. Although the heat input in laser welding is low, significant microstructural changes have been observed due to recovery and recrystallization of the grains in the weld and the heat-affected zone (Ref 7, 8).

Recently, few studies were carried out to evaluate the weldability of magnesium alloys. The relationship between material flow and defects formation during friction stir welding of AZ31 magnesium alloy was reported by Zhang et al. (Ref 9). Microstructure and mechanical properties of laser beam-welded AZ31B magnesium alloy was studied by Coelho et al. (Ref 10). Zhu et al. (Ref 11) compared the process characteristics of CO_2 laser and diode laser welding of AZ31 alloy. Sun et al. (Ref 12) compared GTAW and LBW joints of AZ31 magnesium alloy in terms of weld bead formation and microstructural characterization. However, a detailed comparison has not yet been reported on tensile properties of GTAW, FSW, and LBW joints of AZ31B magnesium alloy. Hence, this article is aimed to reveal the influences of these three welding processes on microstructure, hardness, and tensile properties of AZ31B magnesium alloy.

2. Experimental Work

The rolled plates of AZ31B magnesium alloy were machined to the required dimensions ($300 \times 150 \times 6$ mm^3). The chemical composition and mechanical properties of base metal are presented in Tables 1 and 2. Square butt joint

G. Padmanaban and **V. Balasubramanian**, Center for Materials Joining & Research (CEMAJOR), Department of Manufacturing Engineering, Annamalai University, Annamalainagar 608 002, Tamil Nadu, India; and **J.K. Sarin Sundar**, Centre for Laser Processing of Materials, International Advanced Research Centre for Powder Metallurgy and New Materials (ARCI), Hyderabad 500 005, India. Contact e-mails: gknaban@rediffmail.com, visvabalu@yahoo.com, sarinjk@gmail.com.

configuration, as shown in Fig. 1, was prepared to fabricate the joints. The plates to be joined were mechanically and chemically cleaned by acetone before welding to eliminate surface contamination. The direction of welding was normal to the rolling direction. Necessary care was taken to avoid joint distortion and the joints were made by securing the base metal. Single pass welding procedure was applied to fabricate the joints. High-purity (99.99%) argon gas was used as shielding gas in GTA welding. A nonconsumable, rotating tool made of high-carbon steel was used to fabricate FSW joints. The welding conditions and the optimized process parameters used to fabricate the joints are presented in Table 3.

The welded joints were sliced (as shown in Fig. 2a) using a power hacksaw and then machined to the required dimensions as shown in Fig. 2(b) and (c). American Society for Testing of Materials (ASTM E8M-04) guidelines was followed for preparing the test specimens. Two different tensile specimens were prepared to evaluate the transverse tensile properties. The smooth (unnotched) tensile specimens were prepared to evaluate yield strength, tensile strength, elongation, and reduction in cross-sectional area. Notched specimens were prepared to evaluate notch tensile strength and notch strength ratio of the joints. Tensile test was carried out using a 100 kN, electromechanical-controlled Universal Testing Machine (UNITEK-94100, FIE-Bluestar, India). The 0.2% offset yield strength was derived from the load-displacement diagram. Vicker's microhardness testing machine (HMV-2T, Shimadzu, Japan) was used for measuring the hardness with a 0.05 kg load. Microstructural examination was carried out using a light optical microscope (MIL-7100, MEJI, Japan) incorporated with an image analyzing software (Metal Vision). The specimens for metallographic examination were sectioned to the required size from the joint comprising weld metal, HAZ, and base metal regions and polished using different grades of emery papers. Specimens were etched with a standard reagent made of 4.2 g picric acid, 10 mL acetic acid, 10 mL diluted water, and 70 mL ethanol to reveal the micro- and macrostructure.

3. Results

3.1 Microstructure

Microstructure of the joints was examined at different locations. The optical micrographs were taken at top, middle, and bottom of the weld region in thickness direction and they are displayed in Fig. 3 to 5. From the micrographs, it is understood that the grains are coarser in the top region whereas the finer grains are seen at the bottom of the weld region, irrespective of the welding processes. Similar observation was made by Afrin et al. (Ref 6) in friction stir welding of AZ31 magnesium alloy. Higher temperature experienced by the top surface of the joint, which is very close to the heat source, may be the reason for formation of larger grains. Similar phenomenon was observed in the adjacent region also.

From the micrographs, it is understood that there is an appreciable difference in grain size (average grain diameter) in the weld and HAZ regions. The base metal contains coarse grains (Fig. 6). The fusion zone of GTAW (Fig. 3a-c) joint contains finer equiaxed grains with intergranular $Al_{12}Mg_{17}$ precipitates (β phase). This may be due to the rapid cooling induced by good thermal conductivity and low thermal capacity of magnesium that hampered the growth of grains in fusion zone. In the HAZ, the grains next to the fusion boundary were found to be grown larger due to the intensive heat and high temperature experienced during welding (Fig. 3d-f). Further away from this zone, the grains were more or less same in size as that of the base metal.

Similarly, the nugget region of FSW joint (Fig. 4a-c) contains very fine, equiaxed grains and this may be due to the dynamic recrystallization that occurred during FSW process. The elongated and deformed grains were observed in the TMAZ region (Fig. 4d-f). This may be due to insufficient deformation strain and thermal exposure of this region. This region is located 3 to 4 mm away from the weld center, where the hardness is low. Similar observation was made by Cavaliere and De Marco (Ref 13) and Wang and Wang (Ref 14).

The microstructure in weld region of LBW joint (Fig. 5a-c) consists of fine equiaxed grains. Furthermore, evidence of a large number of precipitated particles is also observed in the weld region. The reason for the formation of a finer microstructure in the weld region could be the rapid cooling induced by the good thermal conductivity and low thermal capacity of

Table 1 Chemical composition (wt.%) of base metal AZ31B magnesium alloy

Al	Mn	Zn	Mg
3.0	0.20	1.0	Bal.

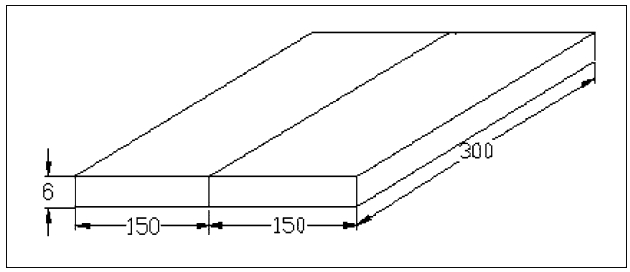

Fig. 1 Dimensions of square butt joint configuration (all dimensions are in mm)

Table 2 Mechanical properties of base metal AZ31B magnesium alloy

Yield strength, MPa	Ultimate tensile strength, MPa	Elongation, %	Reduction in cross-sectional area, %	Notch tensile strength, MPa	Notch strength ratio (NSR)	Hardness (Hv) at 0.05 kg load
171	215	14.7	12.4	192	0.89	69.3

Table 3 Welding conditions and process parameters

Process	GTAW	FSW	LBW
Welding machine	Lincoln, NE	RV Machine Tools, India	Rofin Slab CO_2 laser
Tungsten electrode diameter, mm	3	···	···
Voltage, V	20	···	···
Current, A	180	···	···
Welding speed, mm/min	180	40	5500
Heat input, kJ/mm	0.9	0.54	0.027
Shielding gas	Argon	···	Argon
Gas flow rate, L/min	16	···	20
Tool rotational speed, rpm	···	1600	···
Axial force, kN	···	3	···
Tool pin profile	···	Threaded	···
Tool shoulder diameter, mm	···	18	···
Pin diameter, mm	···	6	···
Pin length, mm	···	5.5	···
Power, W	···	···	2500
Focal position, mm	···	···	−3.0

Mg that inhibited the growth of grains in the weld region. A large number of precipitates ($Al_{12}Mg_{17}$) distributed in the matrix are visible in the weld region which are not observed in the base alloy. Furthermore, there is no distinct HAZ development adjacent to the weld region (Fig. 5d). The macrographs of the joints are displayed in Fig. 7 to display the width and penetration of the joints.

3.2 Lowest Hardness Distribution Profile (LHDP)

Generally, in welded joints, the failure location will be the weakest region (lowest hardness). Almost in all the literature, the hardness profile was measured either along the mid thickness of joint or top surface of the joint to determine the lowest hardness regions. However, it should be pointed out that such hardness profiles could not predict the fracture path of welded joints because of the limited data points. Hence, in this study, the hardness distribution profile is constructed by measuring the hardness at 1 mm interval in thickness direction as well as in transverse direction. It is observed that the fracture paths of welds are consistent with the lowest hardness distribution regions. In GTAW joint (Table 4), reduction in hardness is observed in the HAZ region due to grain coarsening. The lowest hardness of FSW joint (Table 5) is observed in the TMAZ region. Elongated and deformed grains cause softening in this region which may be the reason for reduction in hardness. Appreciable reduction in hardness at the fusion boundary is also observed in the LBW joints (Table 6). The annealing softening in these regions may be the reason for decreased hardness. The lowest hardness distributions in the above regions are confirmed with the fracture path of the tensile specimens (Fig. 8a-f).

Irrespective of the welding processes, the lowest hardness is observed at the top region of the weld region and HAZ. Higher temperature (top region) very near to the heat source led to formation of larger grains due to slow cooling and this may be one of the reasons for lower hardness at the top region of the joints.

3.3 Tensile Properties

The transverse tensile properties such as yield strength, tensile strength and percentage of elongation, notch tensile strength, and notch strength ratio of AZ31B magnesium alloy joints were evaluated. In each condition, three specimens were tested and the average of three results is presented in Table 7. Photographs of welded joints and tensile specimens are displayed in Fig. 9. The tensile curves of unwelded parent metal and welded joints are displayed in Fig. 10. The yield strength and tensile strength of unwelded parent metal are 171 and 215 MPa, respectively. But the yield strength and tensile strength of GTAW joints are 148 and 183 MPa, respectively. This indicates that there is a 15% reduction in strength values due to GTA welding. Similarly, the yield strength and tensile strength of FSW joints are 171 and 208 MPa, respectively, which are 3% lower compared to unwelded parent metal. However, the yield strength and tensile strength of LBW joints are 174 and 212 MPa, respectively. Of the three joints, the joints fabricated by LBW process exhibited higher strength values and the difference is approximately 14% higher compared to GTAW joints and 2% higher compared to FSW joints.

Elongation and reduction in cross-sectional area of unwelded parent metal are 14.7% and 12.4%, respectively. But the elongation and reduction in cross-sectional area of GTAW joints are 7.6% and 5.9%, respectively. This suggests that there is a 48% reduction in ductility due to GTA welding. Similarly, the elongation and reduction in cross-sectional area of FSW joints are 11.8% and 8.7%, respectively, which are 20% lower compared to the parent metal. However, the elongation and reduction in cross-sectional area of LBW joints are 12.1% and 9.4%, respectively. Of the three joints, the joints fabricated by LBW exhibited higher ductility values and the difference is approximately 37% higher compared to GTAW joints and 3% higher compared to FSW joints.

Notch tensile strength (NTS) of unwelded parent metal is 192 MPa, but the notch tensile strength of GTAW joint is 156 MPa. This reveals that the reduction in NTS is approximately 19% due to GTA welding. Of the three joints, the joints fabricated by LBW process exhibited higher NTS values and the difference is 19% higher compared to GTAW and 3% higher compared to FSW. Another notch tensile parameter, NSR, is found to be lesser than unity for all the joints. This suggests that the AZ31B magnesium alloy is sensitive to notches and they fall into the 'notch brittle materials' category. The NSR is 0.89 for unwelded parent metal but it is 0.85 and 0.87 for GTAW and

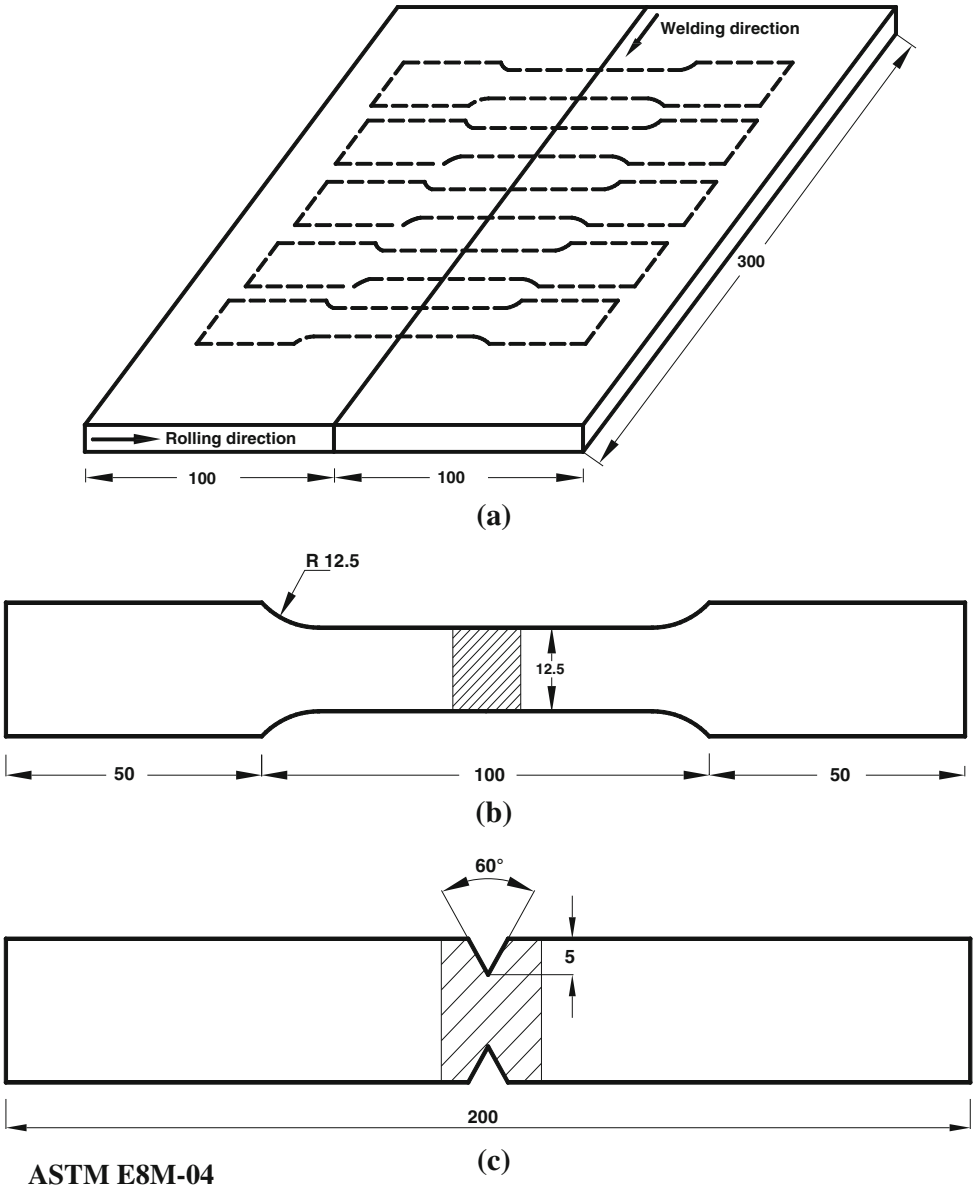

Fig. 2 Dimensions of tensile specimen: (a) Scheme of welding with respect to rolling direction and extraction of tensile specimens, (b) Dimensions of flat smooth tensile specimen, and (c) Dimensions of flat notch tensile specimen

FSW joints, respectively. Of the three joints, the joints fabricated by LBW process exhibited a relatively higher NSR (0.88).

Joint efficiency is the ratio between tensile strength of welded joint and tensile strength of unwelded parent metal. The joint efficiency of GTAW joints is approximately 85% and the joint efficiency of FSW joints is 97%. Of the three joints, the joints fabricated by LBW process exhibited the highest joint efficiency (99%) and it is 14% higher compared to the GTAW joints and 2% higher compared to FSW joints.

4. Discussion

From the tensile test results (Table 7), it could be inferred that the LBW joints are exhibiting superior tensile properties compared to GTAW and FSW joints. During tensile test, GTAW joints failed in the HAZ region and FSW joints failed in the TMAZ region, whereas LBW joints failed in the transition region (Fig. 8).

The grain size of the fusion zone and HAZ are influenced by the heat input of the welding process. Of the three welding processes used in this investigation to fabricate the joints, the GTAW process utilized higher heat input compared to FSW and LBW processes (Table 3). Even though the heat input was high, the reason for the formation of finer microstructure was due to the rapid cooling induced by good thermal conductivity and low thermal capacity of magnesium alloy, which restricted the growth of grains in fusion zone. The microstructure analysis of GTAW revealed coarser grains in HAZ. Fracture was also occurred in HAZ during tensile test. This demonstrates that the HAZ is the weakest link in GTAW joints (Ref 15, 16). This

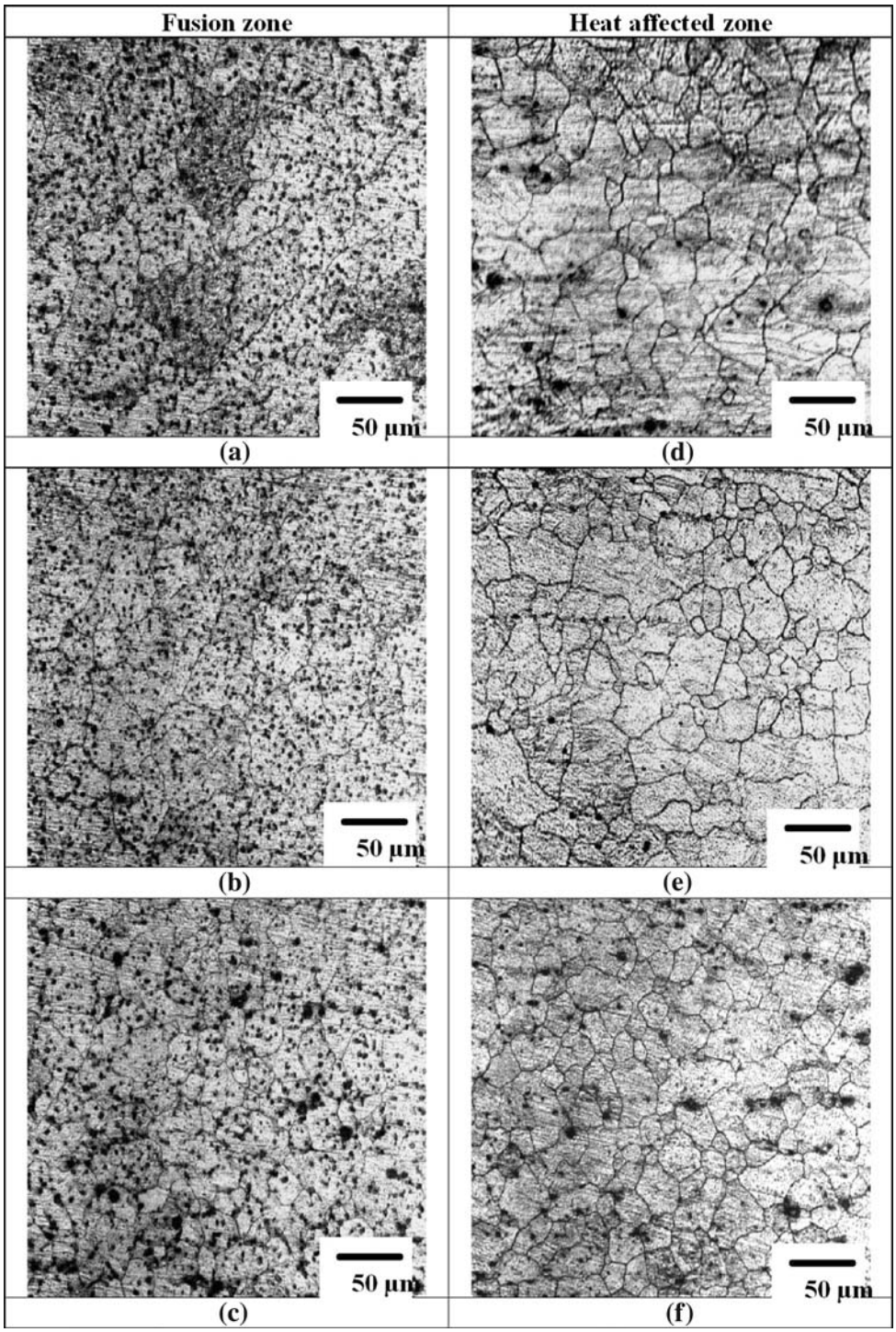

Fig. 3 Optical micrographs of GTAW joint: (a, d) Top region, (b, e) Middle region, and (c, f) Bottom region

may be another reason for the lowest hardness distribution along HAZ of GTAW joints.

In friction stir welding, there is no possibility of formation of a molten weld pool. Due to the frictional heat generated between the tool shoulder and the base metal, the material under the action of the rotating tool attains a plastic state. The axial force applied through the rotating tool causes the plasticized metal to extrude around the tool pin in the vertical direction and get consolidated in the back side when the tool moves forward. Both the stirring and extrusion causes the elongated grains to fragment into smaller grains (Ref 17).

Intense plastic deformation and frictional heating during FSW resulted in generation of fine recrystallized grains in the weld region. The microstructures of nugget region consist of dynamically recrystallized magnesium grains, and intermetallic

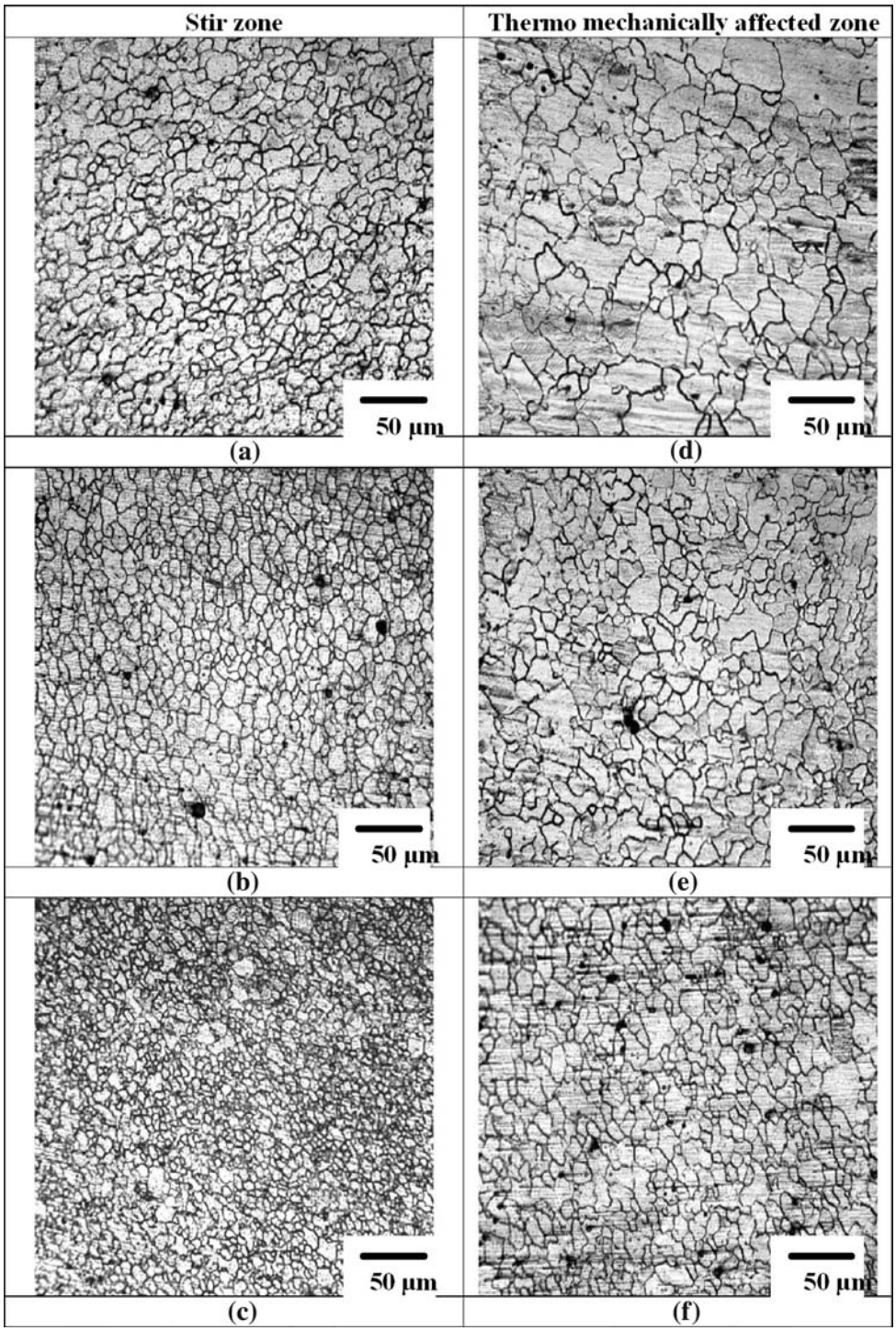

Fig. 4 Optical micrographs of FSW joint: (a, d) Top region, (b, e) Middle region, and (c, f) Bottom region

compounds tend to disappear due to dissolution at elevated temperature (Ref 18). According to the Mg-Al binary phase diagram, $Al_{12}Mg_{17}$ intermetallic compounds in AZ31 will dissolve into the magnesium matrix completely when the heating temperature is higher than a certain value. Therefore, the peak temperature of FSW zone in this study might be high enough for $Al_{12}Mg_{17}$ to dissolve into the magnesium matrix. The grain size of TMAZ is coarser than the nugget region, because of insufficient deformation and thermal exposure (Ref 14). This is also one of the reasons for lowest hardness distribution along TMAZ region in FSW joints.

The microstructure of fusion zone of LBW joint consists of fine equiaxed grains. A large number of precipitates distributed in the matrix are visible in the FZ which are not observed in the base alloy. Due to low heat input and fast cooling, the fusion zone is characterized by very fine grains that resulted in

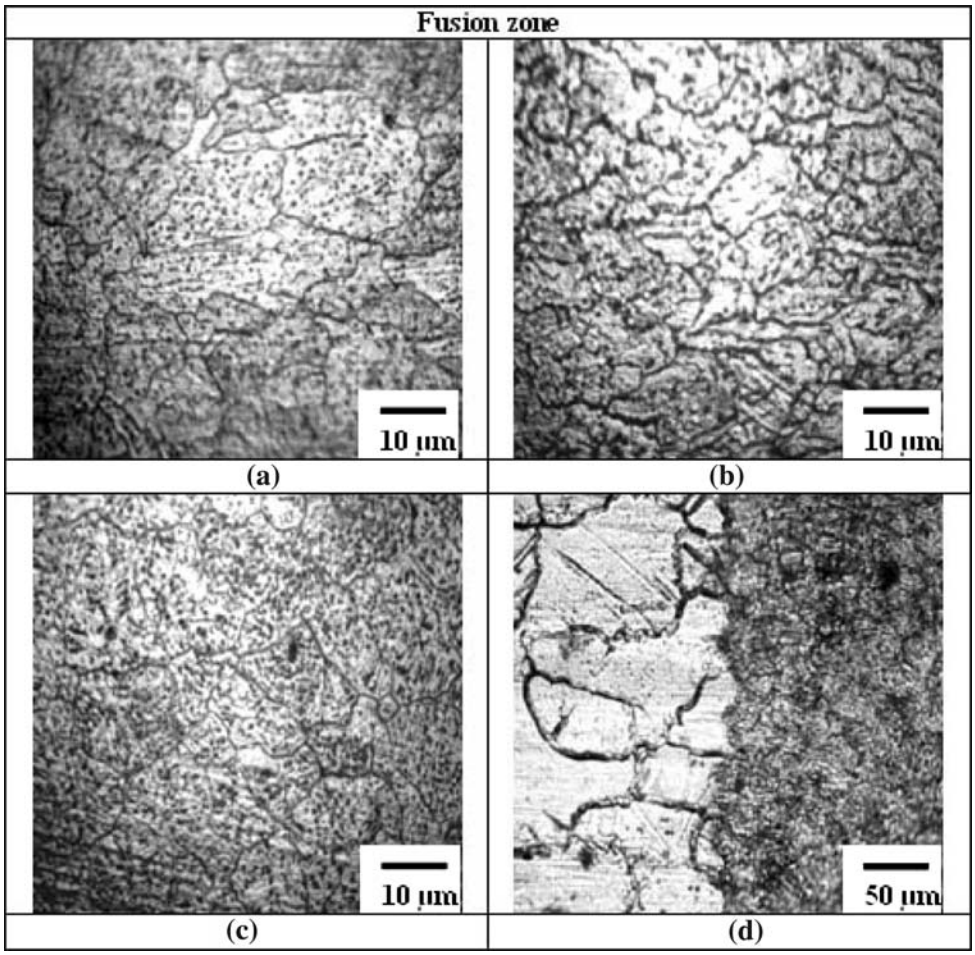

Fig. 5 Optical micrographs of LBW joint: (a) Top region, (b) Middle region, (c) Bottom region, and (d) Transition region

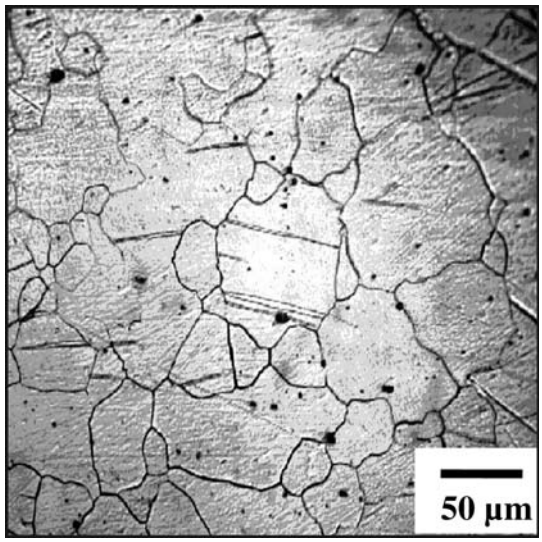

Fig. 6 Optical micrograph of base metal

increase of hardness. Quan et al. (Ref 19) reported that during the laser welding process, the melt alloy is quickly solidified and cooled to room temperature, and the maximum solid solubility of Al decreases immediately from 12.7 wt.% to about 2.0 wt.%. The remnant Al will precipitate the γ-$Mg_{17}Al_{12}$ phase. The sharp transitions from the base metal to the weld region indicate that there is no HAZ and similar observation was made by other investigators also (Ref 20, 21). Appreciable variation in hardness at the fusion boundaries is observed (Table 7). Although heat-affected zone is not observed under optical microscope, it may be present at the fusion boundaries and that may be one of the reasons for variation in hardness at fusion boundaries. At the outset, the annealing softening in these regions might have decreased the hardness (Ref 22).

5. Conclusions

From this investigation, the following important conclusions are derived.

(i) Of the three types of welded joints, the joints fabricated by LBW exhibited higher strength values, and the enhancement in strength was approximately 14% compared to GTAW joints and 2% compared to FSW joints.

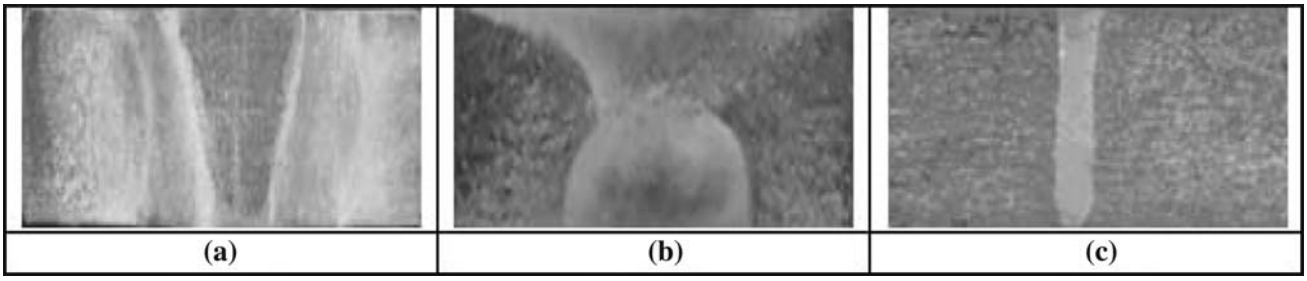

Fig. 7 Macrograph of welded joints (10×). (a) GTAW, (b) FSW, (c) LBW

Table 4 Lowest hardness distribution profile for GTAW joint

Vertical distance, mm (along the thickness direction)	Horizontal distance, mm																			
	−10	−9	−8	−7	−6	−5	−4	−3	−2	−1	0	+1	+2	+3	+4	+5	+6	+7	+8	+9	10
1	73	71	70	71	68	**60**	63	66	68	64	66	65	66	65	68	62	69	71	70	72	72
2	72	72	71	69	**53**	62	65	67	70	69	67	68	70	66	69	68	59	72	72	71	70
3	70	71	73	70	66	**65**	69	68	70	69	69	70	71	73	70	69	69	73	74	70	73
4	73	72	71	71	69	**65**	68	70	69	71	69	69	70	71	68	66	85	76	72	71	70
5	72	71	72	72	70	71	**69**	69	70	71	70	70	72	70	72	70	72	74	72	73	71

Lowest hardness values are in bold

Table 5 Lowest hardness distribution profile for FSW joint

Vertical distance, mm (along the thickness direction)	Horizontal distance, mm																			
	−10	−9	−8	−7	−6	−5	−4	−3	−2	−1	0	+1	+2	+3	+4	+5	+6	+7	+8	+9	10
1	72	70	69	68	66	68	**64**	65	67	66	67	66	66	67	66	70	68	70	72	70	71
2	70	71	69	69	68	72	62	**59**	63	67	68	65	68	63	64	68	69	70	71	72	70
3	72	68	70	71	69	69	62	**60**	63	67	70	68	64	63	65	67	68	69	70	71	69
4	71	69	70	71	69	70	**67**	68	69	70	70	69	68	68	69	70	69	72	73	70	72
5	71	72	70	70	71	72	**70**	71	70	72	72	70	71	72	71	72	72	73	71	71	70

Lowest hardness values are in bold

Table 6 Lowest hardness distribution profile for LBW joint

Vertical distance, mm (along the thickness direction)	Horizontal distance, mm																			
	−5.0	−4.5	−4.0	−3.5	−3.0	−2.5	−2.0	−1.5	−1.0	−0.5	0	0.5	1.0	1.5	2.0	2.5	3.0	3.5	4.0	4.5	5.0
1	72	70	71	69	70	69	68	67	68	**64**	72	66	70	67	66	70	68	70	71	72	70
2	70	72	71	70	69	70	68	68	67	**63**	74	68	70	69	67	68	69	72	71	71	72
3	70	71	72	70	71	69	70	71	73	**65**	75	69	72	69	70	69	68	71	72	71	71
4	71	73	71	70	72	70	69	70	71	**69**	73	71	71	70	69	70	69	71	70	70	72
5	72	71	73	70	71	71	71	72	71	**70**	76	70	71	72	71	72	72	70	70	71	72

Lowest hardness values are in bold

(ii) Hardness was found to be higher in the weld region compared to the HAZ and BM regions, irrespective of welding processes. Very low hardness was recorded in the GTAW joints (70 Hv) and maximum hardness was recorded in the LBW joints (76 Hv).

(iii) The formation of very fine grain microstructure, higher fusion zone hardness, and the absence of heat-affected zone are the main reasons for superior tensile properties of LBW joints compared to GTAW and FSW joints.

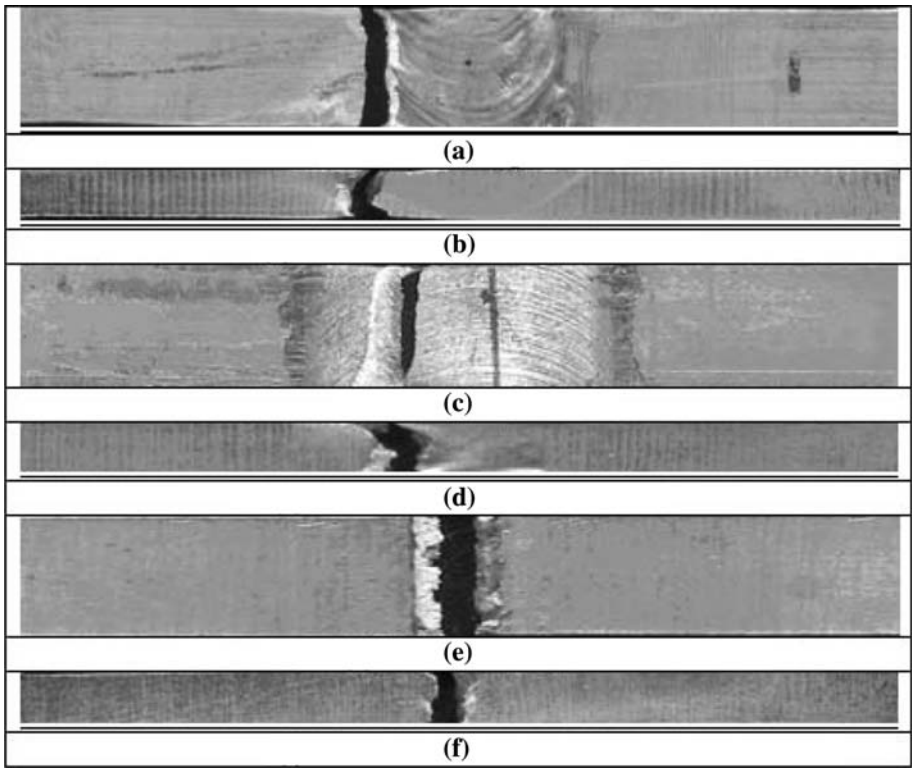

Fig. 8 Failure path in tensile specimens: (a), (c), and (e) represents top view of GTAW, FSW, and LBW, respectively. (b), (d), and (f) represents cross-sectional view of GTAW, FSW, and LBW, respectively

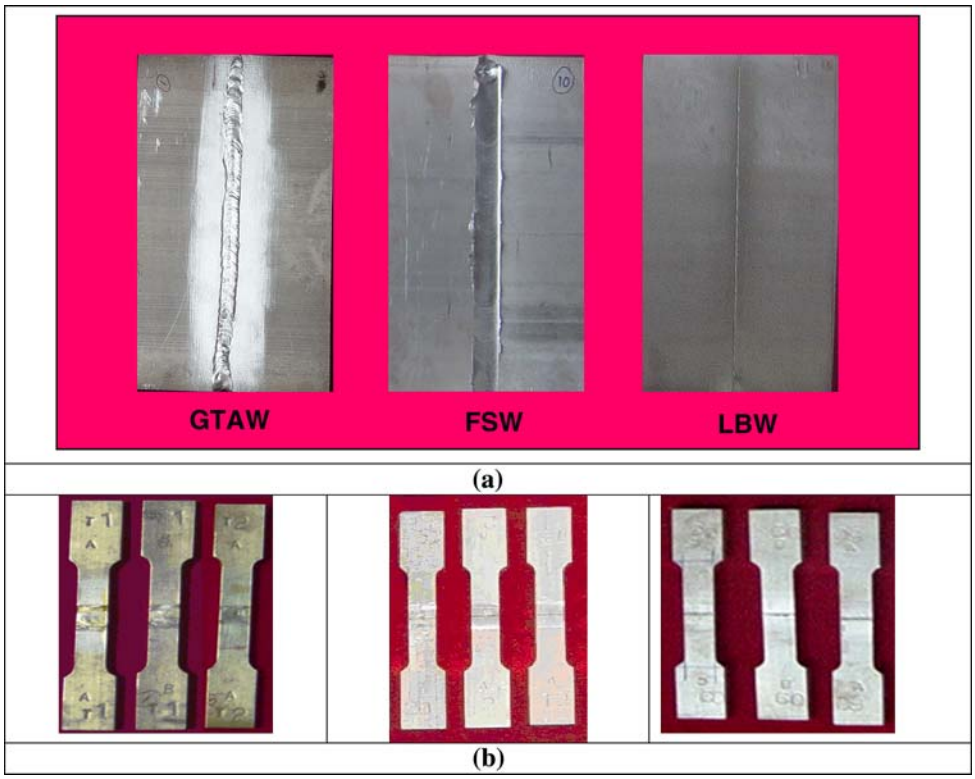

Fig. 9 Photographs of welded joints and respective tensile specimens: (a) Welded joints and (b) Tensile specimens

Table 7 Transverse tensile properties of welded joints

Joint type	Yield strength, MPa	Ultimate tensile strength, MPa	Elongation, %	Reduction in c.s.a, %	Notch tensile strength, MPa	Notch strength ratio (NSR)	Joint efficiency, %
GTAW	148	183	7.6	5.9	156	0.85	85
FSW	171	208	11.8	8.7	181	0.87	97
LBW	174	212	12.1	9.4	187	0.88	99

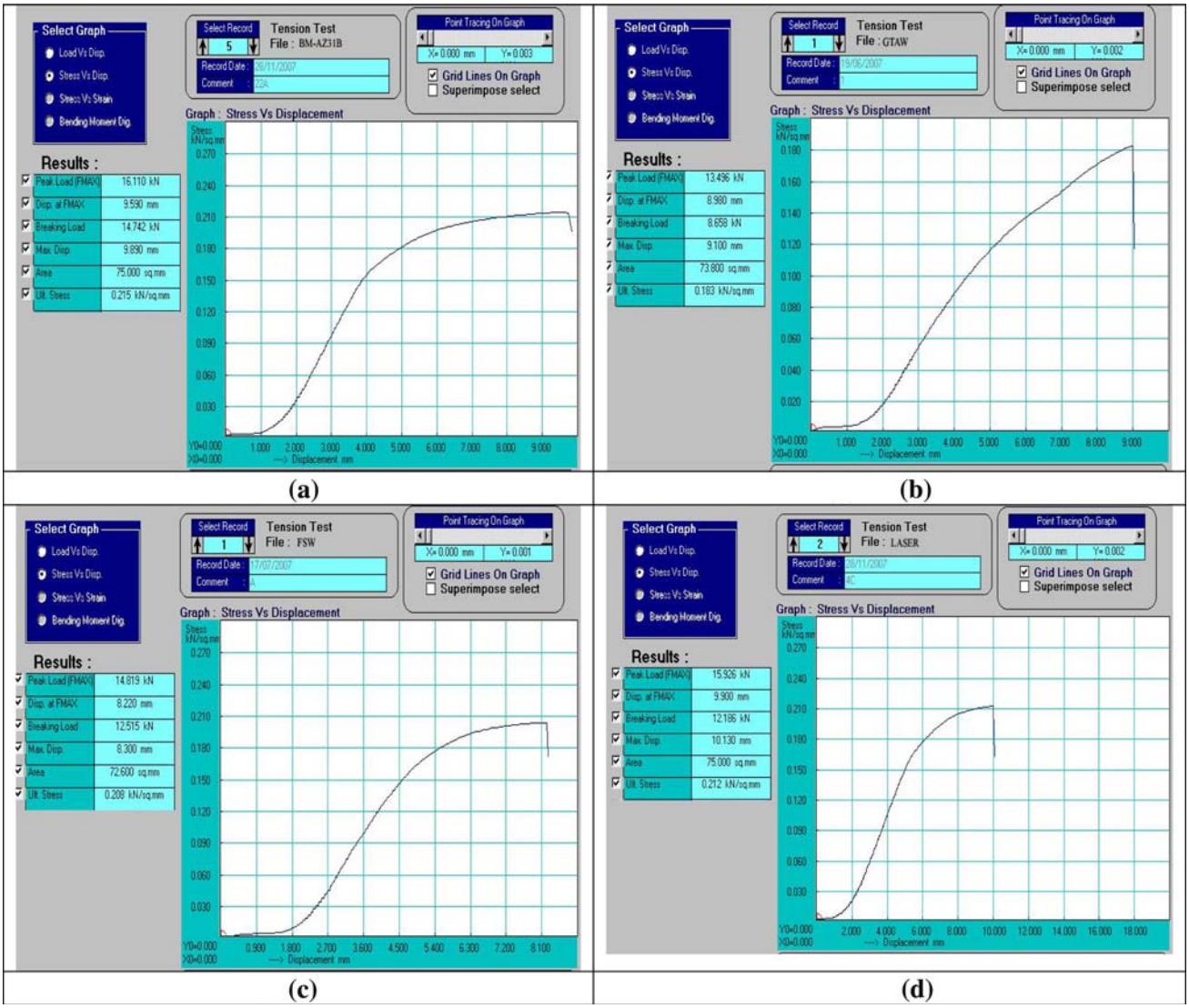

Fig. 10 Tensile curves of unwelded and welded specimens: (a) Base metal, (b) GTAW, (c) FSW, and (d) LBW

Acknowledgments

The authors are grateful to the Department of Manufacturing Engineering, Annamalai University, Annamalai Nagar, India for extending the facilities of Metal Joining Laboratory and Material Testing Laboratory to carryout this investigation. The authors wish to place their sincere thanks to Science and Engineering Research Council (SERC), Department of Science and Technology (DST), New Delhi for financial support rendered through a R&D project no. G5/9167/2005.

References

1. Z.B. Sajuri, Y. Miyashita, Y. Hosokai, and Y. Mutoh, Fatigue Life Prediction of Magnesium Alloys for Structural Applications, *Int. J. Adv. Eng. Mater.*, 2003, **5**(12), p 910–916
2. H. Herold, S. Zahariev, and S. Juttner, Recent Advances in Arc Welding of Magnesium Alloys, *Proceedings of Eurojoin 4*, May 24-26, 2001 (Cavtat-Dubrovnik, Croatia), 2001, p 241–249
3. A. Stern and U. Admon, On the Origin of Beta-Phase Morphology in GTA Welded AZ91Mg Alloy, *Proceedings of Eurojoin 4*, May 24-26, 2001 (Cavtat-Dubrovnik, Croatia), 2001, p 86–95

4. A. Munitz, C. Cotler, A. Stern, and G. Kohn, Mechanical Properties and Microstructure of Gas Tungsten Arc Welded Magnesium AZ91D Plates, *Mater. Sci. Eng. A*, 2001, **302**, p 68–73
5. "Magnesium and Magnesium Alloy," *ASM Specialty Handbook*, ASM International, Materials Park, OH, 1999, p 194–199
6. N. Afrin, D.L. Chen, X. Cao, and M. Jahazi, Microstructure and Tensile Properties of Friction Stir Welded AZ31B Magnesium Alloy, *Mater. Sci. Eng. A*, 2008, **472**, p 179–186
7. K. Behler, J. Berkmanns, and A. Ehrhardt, Laser Beam Welding of Low Weight Materials and Structures, *Mater. Des.*, 1997, **18**, p 261–267
8. E. Schubert, M. Klassen, and I. Zerner, Light-Weight Structures Produced by Laser Beam Joining for Future Applications in Automobile and Aerospace Industry, *J. Mater. Process. Technol.*, 2001, **115**, p 2–8
9. H. Zhang, S.B. Lin, J.C. Feng, and Sh.L. Ma, Defects Formation Procedure and Mathematic Model for Defect Free Friction Stir Welding of Magnesium Alloy, *Mater. Des.*, 2006, **27**, p 805–809
10. R.S. Coelho, A. Kostka, H. Pinto, S. Riekehrb, M. Kocak, and A.R. Pyzalla, Microstructure and Mechanical Properties of Magnesium Alloy AZ31B Laser Beam Welds, *Mater. Sci. Eng. A*, 2008, **485**, p 20–30
11. J. Zhu, L. Li, and Z. Liu, CO_2 and Diode Laser Welding of AZ31 Magnesium Alloy, *Appl. Surf. Sci.*, 2005, **247**, p 300–306
12. Z. Sun, D. Pan, and J. Wei, Comparative Evaluation of Tungsten Inert Gas and Laser Welding of AZ31 Magnesium Alloy, *Sci. Technol. Weld. Join.*, 2002, **7**, p 343–351
13. P. Cavaliere and P.P. De Marco, Superplastic Behaviour of Friction Stir Processed AZ91 Magnesium Alloy Produced by High Pressure Die Cast, *J. Mater. Process. Technol.*, 2007, **184**, p 77–83
14. X.H. Wang and K.S. Wang, Microstructure and Properties of Friction Stir Butt-Welded AZ31 Magnesium Alloy, *Mater. Sci. Eng. A*, 2006, **431**, p 114–117
15. L. Liu and C. Dong, Gas Tungsten-Arc Filler Welding of AZ31 Magnesium Alloy, *Mater. Lett.*, 2006, **60**, p 2194–2197
16. W. Zhou, T.Z. Long, and C.K. Mark, Hot Cracking in Tungsten Inert Gas Welding of Magnesium Alloy AZ91D, *Mater. Sci. Technol.*, 2007, **23**, p 1294–1299
17. K.V. Jata and S.L. Seminatin, Continuous Dynamic Recrystallization During Friction Stir Welding of High Strength Aluminium Alloy, *Scripta Mater.*, 2000, **43**, p 743–749
18. D. Zhang, M. Suzuki, and K. Maruyama, Microstructural Evolution of a Heat-Resistant Magnesium Alloy Due to Friction Stir Welding, *Scripta Mater.*, 2005, **52**, p 899–903
19. Y.J. Quan, Z.H. Chen, X.S. Gong, and Z.H. Yu, Effects of Heat Input on Microstructure and Tensile Properties of Laser Welded Magnesium Alloy AZ31, *Mater. Charact.*, 2008, **59**(10), p 1491–1497. doi: 10.1016/j.matchar.2008.01.010
20. L. Liming, W. Jifeng, and S. Gang, Hybrid Laser-TIG Welding, Laser Beam Welding and Gas Tungsten Arc Welding of AZ31B Magnesium Alloy, *Mater. Sci. Eng. A*, 2004, **381**, p 129–133
21. M. Bobby Kannan, W. Dietzel, C. Blawert, S. Riekehr, and M. Kocak, Stress Corrosion Cracking Behavior of Nd: YAG Laser Butt Welded AZ31Mg Sheet, *Mater. Sci. Eng. A*, 2007, **444**, p 220–226
22. P. Kolodziejczak and W. Kalita, Properties of CO_2 Laser-Welded Butt Joints of Dissimilar Magnesium Alloys, *J. Mater Process Technol.*, 2009, **209**(2), p 1122–1128. doi:10.1016/j.jmatprotec.2008.03.072